Arch. Metall. Mater. **67** (2022), 1, 167-174

DOI: https://doi.org/10.24425/amm.2022.137485

MINGXIANG LIU[1*], SHAN ZHOU[2]

NUMERICAL INVESTIGATION ON THE GAS FIELD GENERATED BY HIGH PRESSURE GAS ATOMIZER FOCUSED ON PHYSICAL MECHANISMS OF GAS RECIRCULATION AND WAKE CLOSURE PHENOMENON

Physical mechanisms of gas recirculation and wake closure were investigated by modeling the gas field generated by High Pressure Gas Atomizer using computational fluid dynamics. A recirculation mechanism based on axial and radial gas pressure gradient was proposed to explain the gas recirculation. The occurrence of wake closure is regarded as a natural result when elongated wake is gradually squeezed by expansion waves of increasing intensity. An abrupt drop could be observed in the numerical aspiration pressure curve, which corresponds well with the experimental results. The axial gradient of gas density is considered as the reason that results in the sudden decrease in aspiration pressure when wake closure occurs. Lastly, it is found that a shorter protrusion length and a smaller melt tip diameter would lead to a smaller wake closure pressure, which could benefit the atomizer design to produce fine metal powder with less gas consumption.

Keywords: Gas field; Aspiration pressure; Recirculation mechanism; Wake closure; Atomization

1. Introduction

Gas atomization of molten metal has become a widely-used process for metal powder manufacturing [1-5], and it is also a critical process of spray forming technology [6-8], in both of which ultrafine and spherical droplets with a narrow size distribution are desired. During the atomization process, the gas field plays a crucial role in determining the size distribution of the droplets obtained after melt's break-up, making it an important part of gas atomization researches.

Of the two main gas atomization processes existing in the powder manufacturing industry, the Close Coupled Gas Atomization (CCGA) process is preferred over the free-fall process, because of the higher atomization efficiency that results from the close proximity of the atomizing gas to the melt delivery tube in CCGA apparatus [9]. A typical gas field generated by a Close Coupled Atomizer is characterized by aspiration pressure and recirculation zone. The aspiration pressure zone, also called negative pressure zone, located below the exit of the melt delivery tube, can help the melt flow into the atomization chamber, and has a close relationship with the breakup of melt. So in order to guarantee a good performing of the atomization process, reasonable negative aspiration pressure is expected in atomization practice. However, this pressure condition at the melt delivery tube can be easily affected by operating parameters and atomizer geometry design [9-15]. D. Schwenck et al. [10] compared the effect of atomizer geometry and atomization pressure on the aspiration pressure between two conventional and a new designed CCGA atomizers. Q. Xu et al. [11] analyzed the variation of aspiration pressure with the inlet gas pressure and protrusion length of melt delivery tube numerically and experimentally. According to their results, a shallow negative or even positive aspiration pressure condition will occur when an unreasonable inlet gas pressure or improper melt delivery tube design is adopted, which usually leads to a failed atomizing implementation. Besides the melt delivery tube design and different types of gas die system can also largely influence the aspiration pressure [12,13], mainly due to different expansion intensity of the gas flow before exiting the gas die.

Another essential characteristic of the CCGA gas field is the gas recirculation zone, an area bounded by melt tip and stagnation point. Inside the recirculation area, the gas flows upstream toward the delivery nozzle from the stagnation point and deflects radially when approaching the nozzle tip. However, when the atomization pressure reaches high enough, the expansion and recompression waves formed by the gas flow after exiting from

[1] SHANGHAI UNIVERSITY, SCHOOL OF MATERIALS SCIENCE AND ENGINEERING, CENTER FOR ADVANCED SOLIDIFICATION TECHNOLOGY, SHANGHAI 200444, CHINA
[2] SHANGHAI JIAO TONG UNIVERSITY, INSTITUTE OF FORMING TECHNOLOGY AND EQUIPMENT, 1954 HUASHAN ROAD, SHANGHAI 200030, CHINA

* Corresponding author: liumx@shu.edu.cn

the nozzle will cross to form a Mach Disk at the centerline of the wake, truncating the recirculation zone and dividing it into two parts, the primary and secondary recirculation zone. Along with the truncation of the wake, an abrupt drop in aspiration pressure appears dramatically during the transition from open to closed wake condition. Ting and Anderson [9] studied the wake evolution under increasing inlet pressure condition, and a closed-wake gas field appears when the inlet pressure reaches a certain value. Also an abrupt decrease in aspiration pressure was observed in their experimental measurements, regardless of the fact that their numerical results of the aspiration pressure is not much well match with the measurements. Motaman et al. [12] investigated the effect of melt delivery tube tip structure with two different gas die systems (cylindrical and C-D die) on the wake closure pressure (WCP), and confirmed a critical inlet pressure value beyond which the wake closure phenomenon would occur.

Even though gas atomization has been widely used for metal powder manufacturing, this method still much relies on empirical operations because physical mechanism of the atomization process remains not thoroughly understood, which is mainly due to the intrinsic complexity of supersonic gas and gas-melt interaction. In the significant work performed by Ting and Anderson, they paid main attention to presenting detailed curves of axial velocity and static pressure under different inlet conditions and discussing the influence of stagnation pressure on aspiration pressure; however, mechanism analysis of some important phenomena existing in the gas field, such as gas recirculation or the abrupt drop of aspiration pressure during the wake closure transition, had not been deeply discussed in their work. So in order to gain a deeper understanding of the mechanisms, a numerical study is performed based on the work of Ting and Anderson. With the calculation results of the gas field generated by a High Pressure Gas Atomizer, the profile evolution of gas field is presented to show how the gas field changes with the inlet pressure, and the gas recirculation mechanism under the melt delivery tube is discussed. Also, the abrupt drop of the aspiration pressure is explained. Furthermore, based on the calculation under different protrusion lengths and melt tip diameters (as shown in Fig. 1), the effect of geometry design on wake closure pressure is studied.

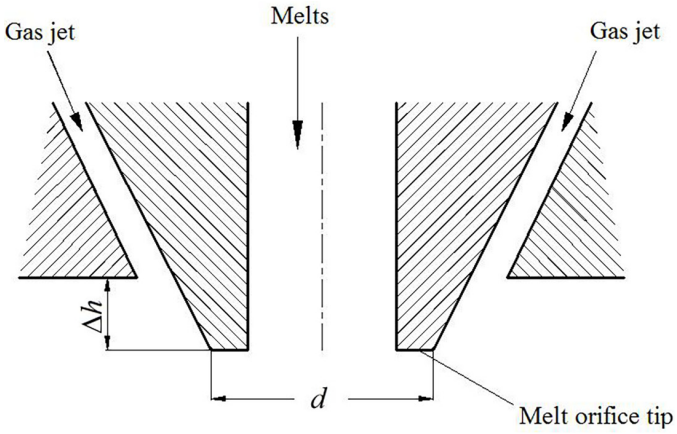

Fig. 1. The cross-sectional view of the HPGA melts feed tube tip geometry

2. Numerical model

The numerical computation was conducted using the commercial CFD software ANSYS Fluent. A gas-only HPGA computational model was constructed based on the dimensions given by Ting and Anderson [9]. In order to capture more gas flow details and reduce the divergence risk under some extreme conditions such as high inlet pressure, a structured quadrilateral mesh was created instead of the unstructured triangular grid as depicted in Fig. 2. Because the atomizer and the whole atomization chamber are axisymmetric, only half of the axial section was calculated.

The standard k-ε turbulent model was adopted to solve the conservative equations of mass, energy and momentum of the gas. A transient calculation method with a time step of 1e-7 s was chosen, and the computation was considered to be convergent when the net mass flow rate decreased to 0.1% of the inlet one. In order to directly compare the calculation results with the experimental and numerical results presented by Ting and Anderson [9], boundary conditions remained the same as the original model of Ting and Anderson, as shown in Fig. 2. Argon with ideal gas properties was used as atomization gas, and a range of gas inlet pressure from 0.69 MPa to 8.0 MPa was

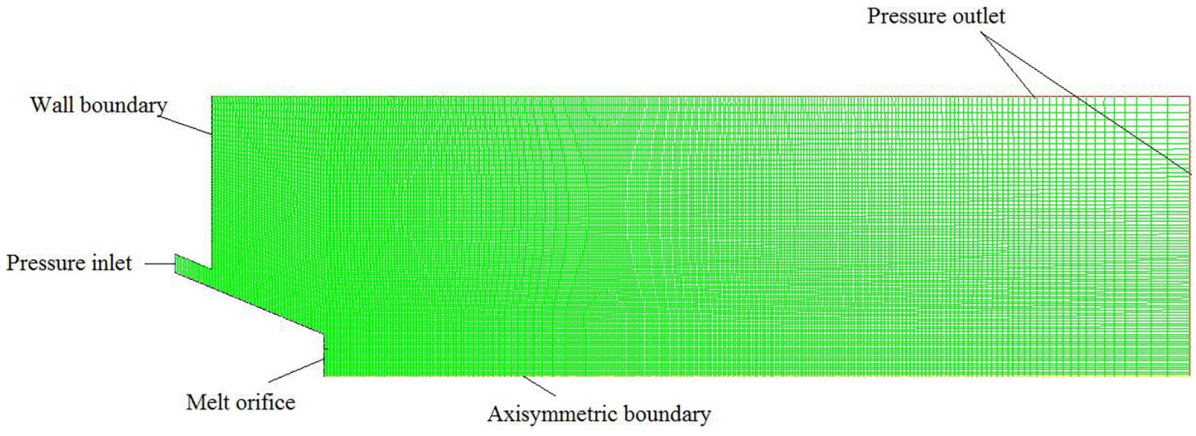

Fig. 2. Schematic drawing of the high pressure gas atomizer computation model

chosen to initialize the inlet pressure of the gas field. For the numerical models that have different protrusion lengths or melt delivery tube tip diameters, the detailed variations of the two parameters are listed in Table 1.

TABLE 1

Parameters Variation of Different Geometry Designs

Parameters	Variation range			
Protrusion Length Δh (mm)	2.55	3.55	4.55*	5.55
Melt Delivery Tube Tip Diameter d (mm)	3.4	5.0	6.6*	8.2

* Underlined numbers are basic dimensions when another parameter varies.

3. Results and discussion

3.1. Recirculation mechanism

The speed vector diagram modelled at an atomization pressure of 0.69 MPa is illustrated in Fig. 3. The blue short arrows represent the speed vectors of different gas elements, and black arrows are marked to show the main recirculation trajectory.

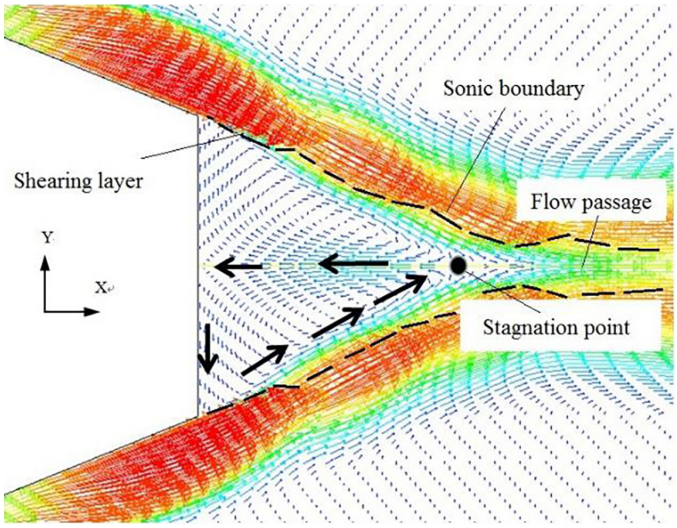

Fig. 3. The vector schematics of the recirculating gas when inlet pressure is 0.69 MPa where black arrows show the direction of gas recirculation

As depicted in Fig. 3, the atomization gas stream can be regarded as a sonic boundary which is hard for low-velocity gas to flow through. Because of the shearing effect of the ultrasonic gas, the gas inside the conical area is disturbed and the gas near the sonic boundary is accelerated and flows till to the cone apex, which is formed due to the combination of the atomization gas stream. Downstream of the cone apex is also occupied by high-velocity gas, and the accelerated gas still in low-velocity state can hardly flow through the narrow passage squeezed by the expansion of the atomization gas. With quite amount of accelerated gas gathering and stopping their flow near the cone apex, the stagnation point with a rather high static pressure forms. On the other hand, with much gas near the sonic boundary sheared and accelerated, the gas density of the area near the melt delivery tube decreases markedly, which gives rise to a sub-ambient pressure condition. Meanwhile, pressure gradient in negative X direction emerges along the axis of the conical area, as shown in the area II in Fig. 4, which drives the gas to flow upward from the stagnation area. And the pressure gradient in positive X direction in area I (Fig. 4) decelerates the recirculating gas and forces it to flow laterally when approaching the melt tip. Therefore, the shearing force from the atomizing gas, together with the axial and radial pressure gradient (depicted in Fig. 6), serves as the driving force that maintains the gas recirculation.

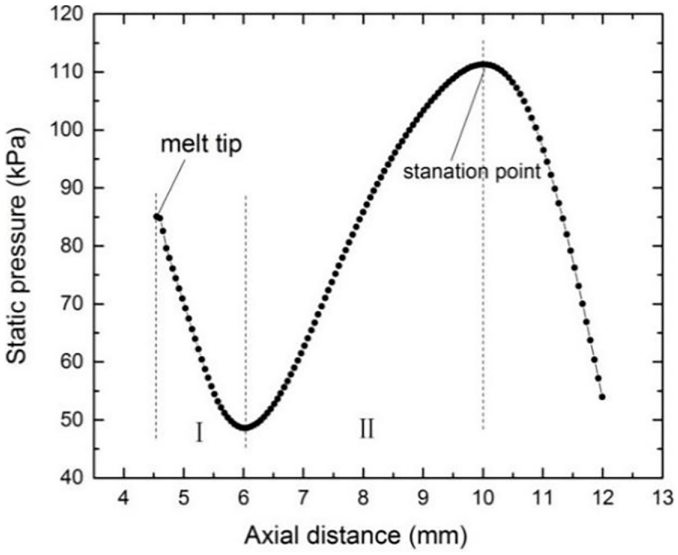

Fig. 4. Gas static pressure along the axis of gas filed when inlet pressure is 0.69 MPa

3.2. Wake evolution with increasing inlet pressure

The four velocity contour images depicted in Fig. 5 show the profiles of gas field under the inlet pressure of 1.50 MPa, 4.40 MPa, 4.50 MPa and 6.60 MPa. For the cylindrical nozzle with atmospheric back pressure, the critical inlet pressure at which the gas will expand completely after exiting the nozzle, can be given according to the conclusion of isentropic flow of compressible gas [16]

$$\frac{P_b}{P_*} = \left(\frac{2}{\kappa+1}\right)^{\frac{\kappa}{\kappa-1}} \tag{1}$$

where P_b is the atmospheric pressure, and κ is the specific heat ratio (for argon κ = 1.66). Then the critical inlet pressure P_* = 0.205MPa can be solved , under or over which the gas would be over-expanded or less-expanded respectively when exiting the nozzle. The four gas field calculations were all performed with a gas inlet pressure over P_*, so the gas exiting the cylindrical nozzle all experienced further expansion upon entering the gas chamber.

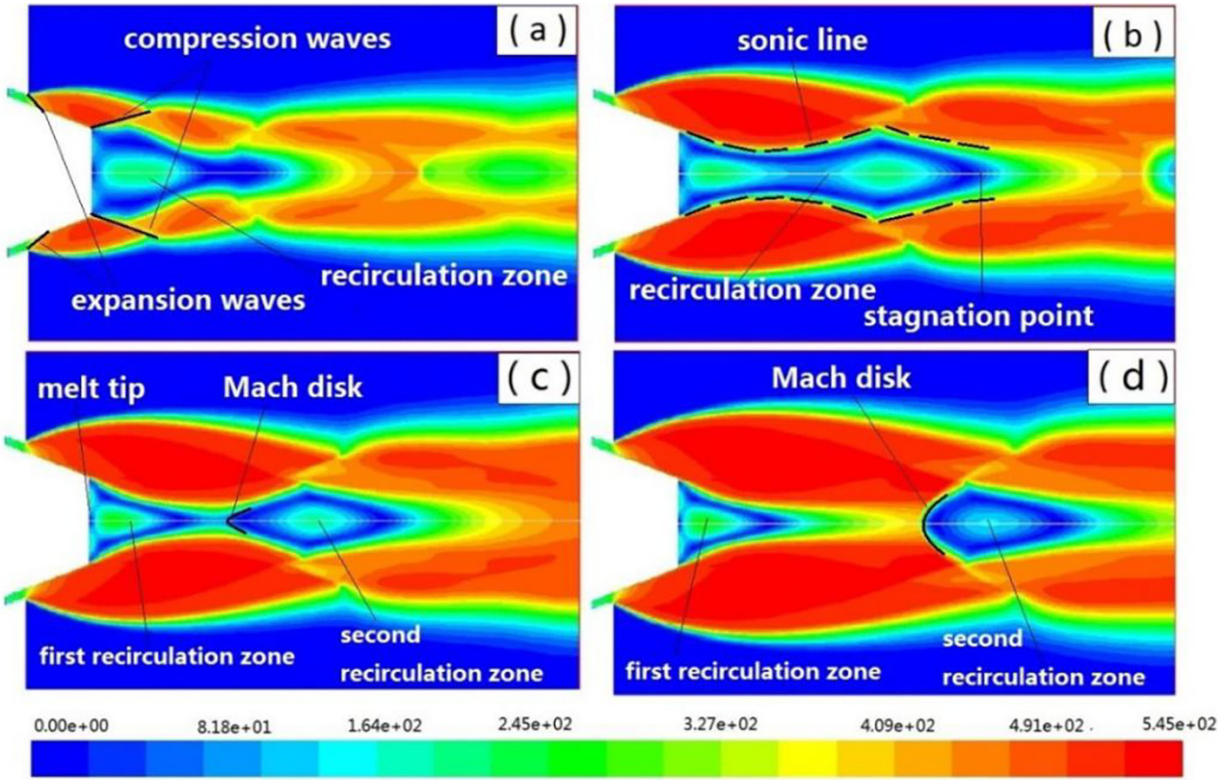

Fig. 5. The velocity contours of the wake profile when the inlet pressure was respectively set as (a) P = 1.50 MPa; (b) P = 4.40 MPa; (c) P = 4.50 MPa; (d) P = 6.10 MPa

When the inlet pressure was 1.50 MPa, as shown in Fig. 5a, the gas streams converged and formed a unified gas flow after experiencing a series of expansion and compression waves, and meanwhile a gas recirculation zone bounded by the melt tube tip, sonic line and the stagnation point occurred downstream the melt delivery tube along the axis of the gas field.

As the inlet pressure was increased to 4.40 MPa, the gas underwent large re-expansion after exiting the gas nozzle and the recirculation zone was lengthened obviously. Due to the strong expansion waves, the wake was squeezed severely to form an arrow-shaped profile as depicted in Fig. 5b. When the inlet pressure was increased to 4.50 MPa, the wake closure phenomenon happened. The recirculation zone was truncated and divided into two parts (Fig. 5c). As the inlet pressure further increased to 6.10 MPa, the whole gas field had a similar wake profile as 4.50 MPa, except that the Mach disk gradually moved away from the melt orifice tip (Fig. 5d).

The profile of the recirculation zone was mainly dominated by the intensity of expansion-recompression waves, which increased with the inlet pressure. And the profile evolution of the recirculation zone depicted in Fig. 5 demonstrates that the occurrence of the wake closure phenomenon is not a sudden transition, but a natural result when the expansion intensity of the gas stream reaches strong enough. However, such natural result, i.e. the occurrence of the Mach disk, can largely change the profile of the recirculation zone and lead to an abrupt decrease of the aspiration pressure, thus deeply affecting the atomization process [17].

3.3. Aspiration pressure variation with inlet pressure

Ting and Anderson [9] have presented the comparison curves of the calculated and measured aspiration pressure results under different inlet pressure condition. However, the wake closure phenomenon which could be represented by a sudden drop in aspiration pressure could hardly observed in their calculated results. A series of gas-only calculations were conducted with different inlet pressure in this study in order to seize and present such abrupt drop in aspiration pressure graph more intuitively.

The static pressure under the melt delivery tube was proved to be non-uniform along radial direction as depicted in Fig. 6. Considering pressure is a synthetic effect of quantities of gas molecules impacting on a certain surface, an area integration method was adopted to calculate the averaged inspiration pressure across the melt delivery tube.

$$\overline{P} = \frac{\int_0^R P(r) 2\pi r dr}{\pi R^2} \tag{2}$$

where $P(r)$ is the static pressure at the point that is r away from the axis. R is the radius of the melt delivery tube.

The numerical aspiration pressure results calculated based on equation (2) were depicted in Fig. 7, together with the computational and experimental results from Ting and Anderson. The numerical results in this study remain a similar trend to their original work. Before the inlet pressure reaching to the critical

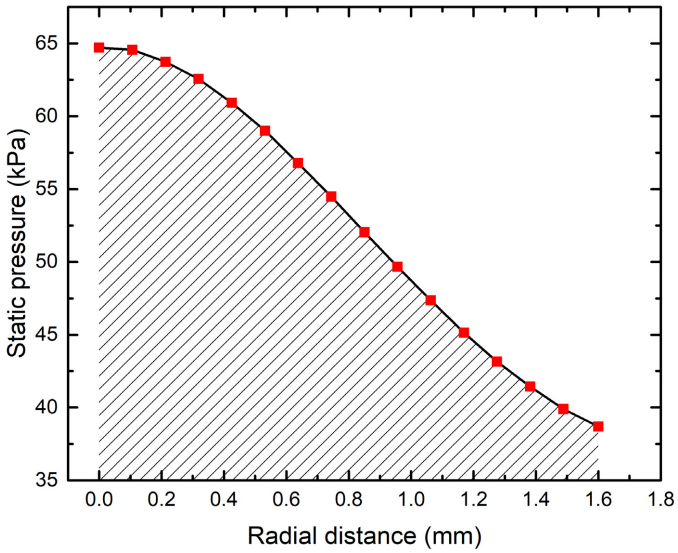

Fig. 6. The calculated radial distribution of static pressure under the melt delivery tube when the inlet pressure is 0.69 MPa

point, the aspiration pressure dropped from an over-ambient condition to a sub-ambient pressure as the inlet pressure increased. The critical points of the inlet pressure were 3.45 MPa and 4.50 MPa respectively in Ting's numerical results and in this study. When the inlet pressure crossed the critical point, the aspiration pressure increased gradually with the increase of the inlet pressure. Compared with Ting's numerical results, it is inspiring to observe the clear abrupt drop in aspiration pressure when the inlet pressure is 4.50 MPa, which corresponds with the wake-closure transition as shown in Fig. 5c. However, some gaps still exist between the numerical results and the experimental measurements. The wake closure transition occurs earlier (4.50 MPa) compared with the experimental results (about 5.50 MPa), and the decrease in aspiration pressure is 20 kPa at the transition point, about 10 kPa less than the measured result

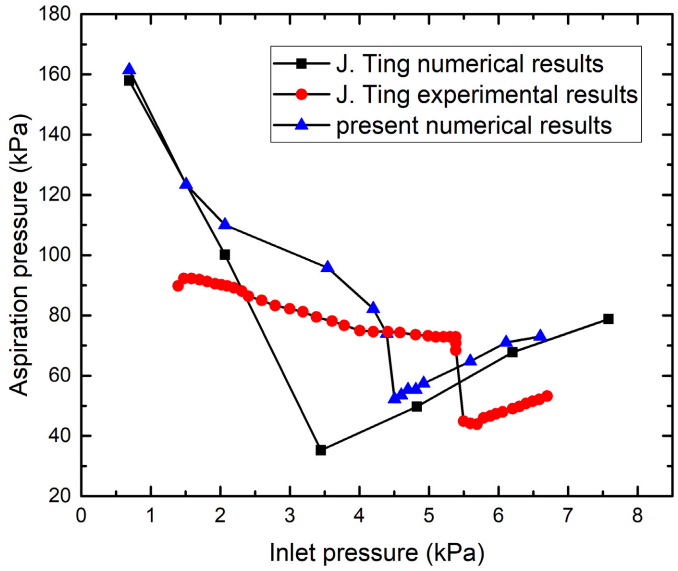

Fig. 7. Computational and experimental results of the aspiration pressure under different inlet pressure

(near 30 kPa). Apart from the inaccuracy of the numerical model, the reason leading to such gaps probably lies in the difference between the exit area of the calculated model and the experimental atomizer.

In addition, the numerical results in this study show better agreement with J. Ting's experimental results [9]. This is mainly attributed to the difference in meshing strategies. The refinement structural grid method brings about the improved accuracy of the simulation results. Of course the difference in fluid model may also be the reason, but hard to discuss in details due to the lack of the model data. However, it is sure that this work indicates the ability of the standard k-ε turbulent model to be applied in the supersonic nozzles.

3.4 Explanation for the abrupt drop in aspiration pressure

It has been reported [17] that the median powder size could show a decrease as large as 42% when the operation pressure increases no more than 0.05 MPa (from an open wake condition to a closed wake condition). The abrupt drop in aspiration pressure during the wake closure transition contributes to that dramatic decrease. The relationship between the aspiration pressure and the yielding metal powder size is not discussed in the paper. However, some efforts have been taken in this study to figure out what leads to the sudden occurrence of the abrupt decrease in aspiration pressure.

As shown in Fig. 8a, an evident density gradient exists along the axis of the gas field. Considering the gas static pressure is proportional to its density, such density gradient is consistent with the axial pressure gradient. The gas density curves in Fig. 8a indicate that when inlet pressure is increased from 4.20 MPa to 4.40 MPa, or from 4.50 MPa to 4.70 MPa, the gas density along the axis doesn't show an obvious change; however, when inlet pressure is increased from 4.40 MPa to 4.50 MPa, a much bigger density peak can be observed in latter density curve, and for the area from 4.5 to about 11 mm in axial direction, the gas density shows an apparent drop. When it comes to the radial gas density just below the melt delivery tube, a similar trend can be observed from Fig. 8b. Radial gas density changes slightly when inlet pressure is increased from 4.20 MPa to 4.40 MPa or from 4.50 MPa to 4.70 MPa, but drops largely from 4.40 MPa to 4.50 MPa. The axial velocity curves depicted in Fig. 8c clearly shows that the whole recirculation zone is separated into two parts when the inlet pressure is increased from 4.40 MPa to 4.50 MPa, which means that the wake closure occurs, and the first recirculation zone ranges from 4.5 to about 11 mm, just corresponding to the area that undergoes an apparent drop in axial gas density during the wake closure transition.

So based on the above analysis, the reason resulting in the abrupt drop of aspiration pressure during the wake closure transition can be given as follows. An obvious gradient exists in the density distribution curve along the axis, and near the stagnation point gathers relative dense gas. When the wake closure transi-

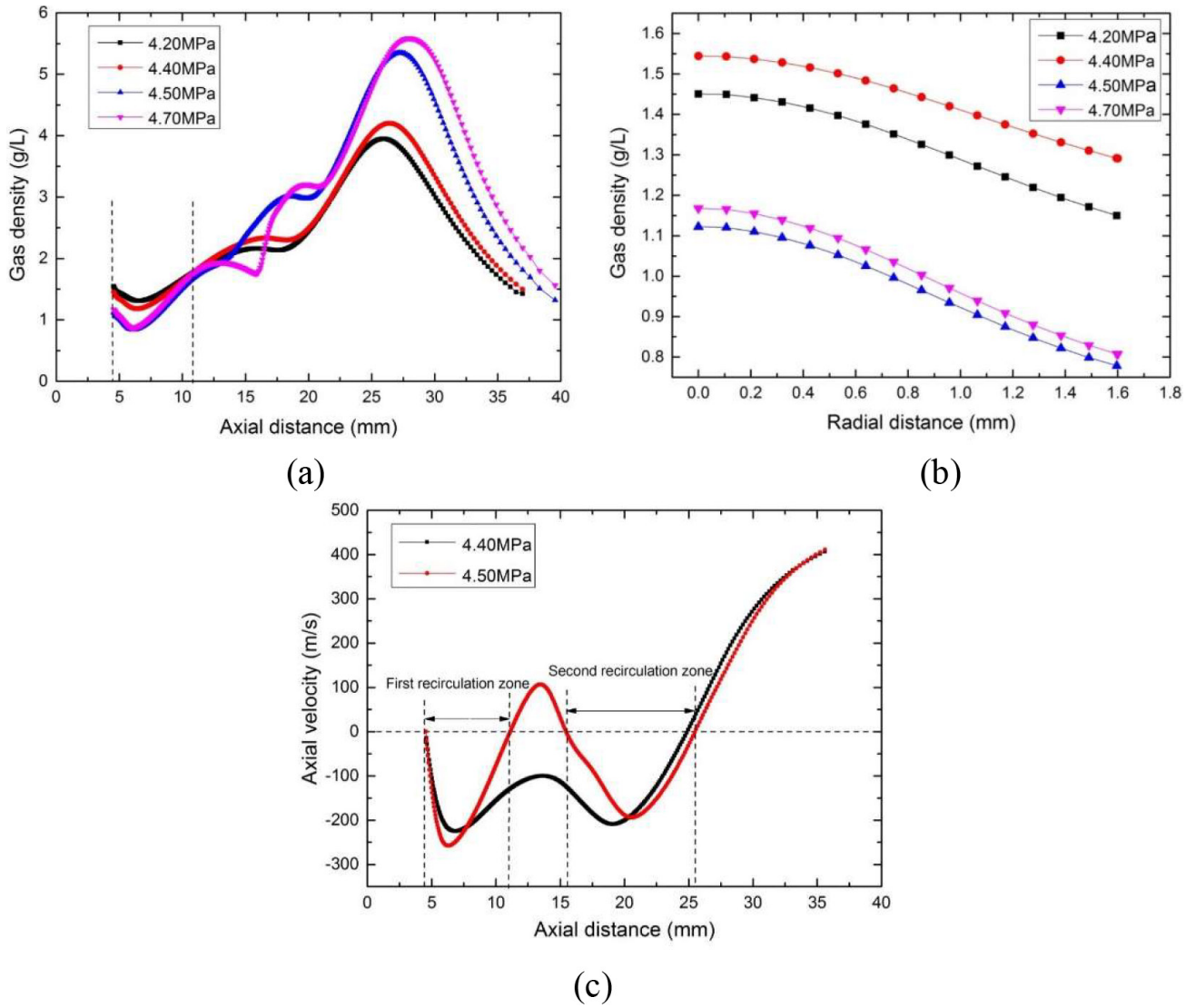

Fig. 8. Comparison of the gas density and velocity distribution curves before and after the wake-closure transition: (a) axial gas density, (b) radial gas density, (c) axial gas velocity

tion occurs, the recirculation zone is truncated and divided into two parts, and the high-density gas is restricted to the second recirculation area, because the gas can not flow through the Mach disk. As a consequence, only low-density gas remains to recirculate in the first recirculation zone, which directly results in the sudden decrease of gas density in the first recirculation zone, and thus leading to the abrupt drop of static pressure near the melt delivery tube.

3.5. WCP variation with protrusion length and melt delivery tube tip diameter

The protrusion length of delivery tube and melt delivery tube tip diameter are important factors that influence aspiration pressure condition [11,18]. The aspiration pressure curves for different protrusion lengths depicted in Fig. 9 share a common variation trend. The aspiration pressure decreases with the inlet pressure before the wake closure transition, and when the inlet pressure increases to reach the WCP, the aspiration pressure drops abruptly, followed by a rise trend when inlet pressure further increases. It is also demonstrated in Fig. 9 that the WCP increases with the protrusion length, 3.3 MPa, 3.9 MPa, 4.5 MPa and 5.1 MPa when the protrusion length is 2.55 mm, 3.55 mm, 4.55 mm and 5.55 mm respectively. And when the wake closure transition happens, a longer protrusion length leads to a deeper sub-ambient aspiration pressure. What's more, before the wake closure transition, a deeper sub-ambient aspiration pressure can be obtained by a shorter protrusion; while after the wake closure transition, the aspiration pressure rises more rapidly for the shorter protrusion.

The wake closure is regarded as a natural result when the expansion intensity of the gas stream reaches strong enough to cross and combine together at the axis of the gas field. Based on such explanation, it can be expected that a smaller diameter of melt delivery tube tip will lead to a smaller WCP, because weaker expansion intensity is needed for the gas streams to cross each other when the annular gas streams exit from

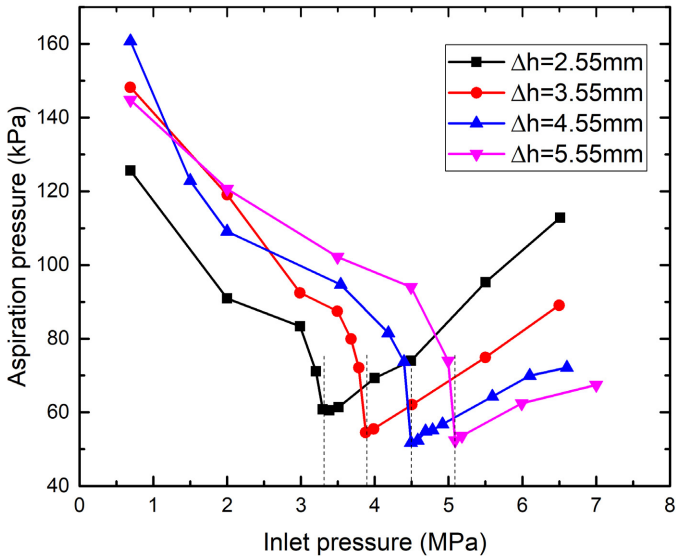

Fig. 9. Aspiration pressure variation curves with inlet pressure under different protrusion lengths

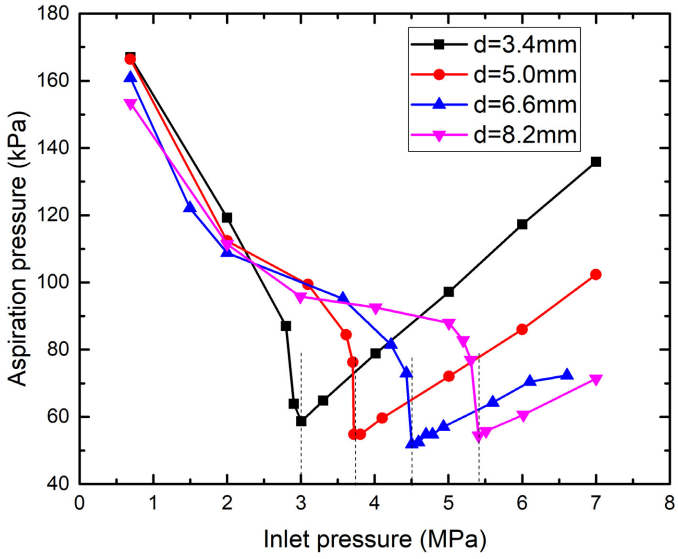

Fig. 10. Aspiration pressure variation curves with inlet pressure under different melt delivery tube tip diameters

a smaller-diameter delivery tube, and vice versa. The numerical results depicted in Fig. 10 confirm the expectation above, the WCPs for the tip diameter of 3.4 mm, 5.0 mm, 6.6 mm and 8.2 mm are 3.0 MPa, 3.70 MPa, 4.50 MPa and 5.40 MPa respectively.

The four aspiration pressure curves under melt delivery tube tip diameters in Fig. 10 also show a same variation trend with that of different protrusion lengths. Before the wake closure transition, the aspiration pressure decreases rapidly with the inlet pressure, and when the WCP is reached, the aspiration pressure drops abruptly, followed by a rise trend when inlet pressure further increases. The aspiration pressure at the wake closure transition shows a slight decrease when melt delivery tube tip diameter increases, and the aspiration pressure rises more rapidly for a smaller melt delivery tube tip structure.

Ting et al. [17] has pointed out that atomizing at the pressure above WCP indeed produce finer powder but at the expense of higher gas consumption compared with below WCP atomization. Therefore, a lower WCP is preferred to reduce the gas consumption. On the other hand, gas-melt mass flow rate (GMR) which is associated with the inlet pressure is believed to deeply influence the yielding powder size. Fine powder can hardly be obtained by low GMR atomization even if at pressure above WCP. So both the WCP and the GMR have to be considered when choose the proper operation pressure, protrusion length and melt tip diameter, which can draw guidance from the numerical results shown in Fig. 9 and Fig. 10.

4. Conclusions

By means of numerical calculation, this study provided an insight into the important physical mechanisms existing in HPGA gas filed. The profile evolution of the gas field with inlet pressure was presented, which indicated that the occurrence of the wake closure is a natural result when the recirculation zone is gradually elongated and squeezed by expansion waves.

By adopting an integral method, the aspiration pressure was calculated across the whole melt delivery tube area. An abrupt drop of the aspiration pressure could be clearly observed from the aspiration pressure curve, which shows better coincidence with the experimental results from Ting and Anderson compared with their computation.

Based on the axial and radial pressure gradient, a recirculation mechanism containing gas shearing effect was proposed to explain the gas recirculation. The axial gradient of gas density is considered to be the reason that results in the sudden drop of the aspiration pressure when the wake closure phenomenon occurs. Because high-density gas near the stagnation point is restricted inside the secondary recirculation zone after the wake is truncated, leaving thin gas recirculating within the first recirculation zone.

The numerical calculation of the wake closure pressure variation with protrusion length and melt tip diameter was also performed. For HPGA atomizer, a shorter protrusion length and a smaller melt tip diameter would lead to a smaller WCP; the WCPs are 3.3 MPa, 3.9 MPa, 4.5 MPa and 5.1 MPa when the protrusion length is 2.55 mm, 3.55 mm, 4.55 mm and 5.55 mm respectively and 3.0 MPa, 3.70 MPa, 4.50 MPa and 5.40 MPa corresponding to the melt tip diameter of 3.4 mm, 5.0 mm, 6.6 mm and 8.2 mm. These conclusions will benefit the HPGA atomizer design when lower WCP is desired to produce fine powder with less gas consumption.

Acknowledgements

The authors are very grateful to Prof. Zhenshan Cui and Associate Prof. Dashan Sui in Shanghai Jiao Tong University for their guidance and supervision on this work.

Declaration of Competing Interest

The authors declare that there are no known financial interests or personal relationships that could have appeared to influence the work in this paper.

REFERENCES

[1] K. Kassym, A. Perveen, Mater. Today Proc. **26**, 1727-1733 (2020).

[2] A.M. Mullis, L. Farrell, R.F. Cochrane, N.J. Adkins, Metall. Mater. Trans. B **44** (4), 992-999 (2013).

[3] D. Beckers, N. Ellendt, U. Fritsching, V. Uhlenwinkel, Adv. Powder Technol. **31**(1), 300-311 (2020).

[4] B. Zheng, Y. Lin, Y. Zhou, E.J. Lavernia, Metall. Mater. Trans. B **40** (5), 768-778 (2009).

[5] N. Zeoli, S. Gu, Comput. Mater. Sci. **38** (2), 282-292 (2006).

[6] S. Hussain, C. Cui, L. He, L. Mädler, V. Uhlenwinkel, J. Mater. Process. Technol. **282** (116677), 1-8 (2020).

[7] G.S.E. Antipas, Powder Metall. **56** (4), 317-330 (2013).

[8] M. Jeyakumar, G.S. Gupta, S. Kumar, J. Mater. Process. Technol. **203** (1/3), 471-479 (2008).

[9] J. Ting, I.E. Anderson, Mater. Sci. Eng. A **379** (1-2), 264-276 (2004).

[10] D. Schwenck, N. Ellendt, J. Fischer-Bühner, P. Hofmann, V. Uhlenwinkel, Powder Metall. **60** (3), 198-207 (2017).

[11] Q. Xu, D. Cheng, G. Trapaga, N. Yang, E.J. Lavernia, J. Mater. Res. **17** (1), 156-166 (2002).

[12] S. Motaman, A.M. Mullis, R.F. Cochrane, D.J. Borman, Metall. Mater. Trans. B **46** (4), 1990-2004 (2015).

[13] C. Cui, F. Cao, Q. Li, J. Mater. Process. Technol. **137** (1-3), 5-9 (2003).

[14] O. Aydin, R. Unal, Comput. Fluids **42** (1), 37-43 (2011).

[15] R. Kaiser, C. Li, S. Yang, D. Lee, Adv. Powder Technol. **29** (3), 623-630 (2018).

[16] G.S.E. Antipas, Comput. Mater. Sci. **46** (4), 955-959 (2009).

[17] J. Ting, M.W. Peretti, W.B. Eisen, Mater. Sci. Eng. A **326** (1), 110-121 (2002).

[18] A. Aksoy, R. Ünal, Powder Metall. **49** (4), 349-354 (2006).